

**NOVEL APPROACH IN STATIC SHIFT
CORRECTION FOR MAGNETOTELLURICS
DATA USING 2D ELECTRICAL RESISTIVITY
IMAGING**

MUHAMMAD NAZRIN BIN A RAHMAN

UNIVERSITI SAINS MALAYSIA

2022

**NOVEL APPROACH IN STATIC SHIFT
CORRECTION FOR MAGNETOTELLURICS
DATA USING 2D ELECTRICAL RESISTIVITY
IMAGING**

by

MUHAMMAD NAZRIN BIN A RAHMAN

**Thesis submitted in fulfilment of the requirements
for the degree of
Doctor of Philosophy**

May 2022

ACKNOWLEDGEMENT

Alhamdulillah. I would like to express my sincere gratitude to my main supervisor, Prof. Madya Dr. Nordiana Mohd Muztaza for the continuous support, patience, motivation and funding throughout my PhD candidature. Thank you for every chance given for me to learn more about research field. My gratitude also goes to my co-supervisors Prof Dr. Rosli Saad and Dr. Teoh Ying Jia for ideas and guidance throughout the research. My heartfelt gratitude goes to my lovely wife, Dr. Najmiah Rosli for her non-stop moral support and encouragement, contributing rational ideas and lot of discussions especially in geological knowledge until this thesis can be successfully done. Thank you to geophysics team from Universiti Sains Malaysia (USM) for for sacrificing their time and energy assisting me in the projects especially during data acquisition. Special thanks to Mineral and Geoscience Department Malaysia (JMG) for allowing me to make use of the data, for all assists during data acquisition and for lending geophysics equipment. I hope collaboration of this kind, will further in the future. Further and the most important, million thanks to my parents A Rahman Talib and Siti Hamidah Ishak, my siblings Mohammad Haikal, Nazirah, Nadira and Najihah for their prayers, support and understanding during my study. Thank you to Ministry of Higher Education Malaysia for Fundamental Research Grant Scheme with Project Code: FRGS/1/2018/STG09/USM/03/2 entitle 'Development of 2-D linear inversion algorithm from geophysical approach for soil or rock characteristics' and also Research University grant entitle 'Integrated geophysical characterization of geothermal exploration and strategy for a sustainable use of geothermal resources' with account no. 1001/PFIZIK/8011110.

TABLE OF CONTENTS

ACKNOWLEDGEMENT	ii
TABLE OF CONTENTS	iii
LIST OF TABLES	vi
LIST OF FIGURES	vii
LIST OF SYMBOLS	xiii
LIST OF ABBREVIATIONS	xiv
ABSTRAK	xv
ABSTRACT	xvii
CHAPTER 1 INTRODUCTION	1
1.1 Background	1
1.2 Problem statement.....	2
1.3 Research objectives.....	3
1.4 Scope of study	3
1.5 Novelty.....	4
1.6 Thesis layout	4
CHAPTER 2 LITERATURE REVIEW	6
2.1 Introduction	6
2.2 Electromagnetic (EM) sources.....	6
2.3 Transfer function.....	8
2.4 Dimensionality	10
2.4.1 1D Earth.....	11
2.4.2 2D Earth.....	12
2.4.3 3D Earth.....	13
2.5 Static shift.....	14
2.5.1 Static shift sources	15

2.5.2	Static shift correction	19
2.6	2D electrical resistivity imaging	25
2.7	Chapter summary	30
CHAPTER 3 METHODOLOGY		32
3.1	Introduction	32
3.2	Regional geology	33
3.3	2D electrical resistivity imaging	34
3.3.1	Apparent resistivity	35
3.3.2	True resistivity	36
3.4	Magnetotellurics.....	37
3.5	Static shift correction	40
3.6	Chapter summary	43
CHAPTER 4 RESULT AND DISCUSSION		44
4.1	Introduction	44
4.2	2D electrical resistivity imaging	44
4.2.1	Apparent resistivity	45
4.2.2	True resistivity	48
4.3	Magnetotellurics.....	52
4.4	Static shift correction	56
4.4.1	Apparent resistivity.....	56
4.4.2	True resistivity.....	62
4.4.3	Analysis.....	67
4.5	MT inversion.....	68
4.6	Chapter summary	76
CHAPTER 5 CONCLUSION AND RECOMMENDATIONS.....		77
5.1	Conclusion.....	77
5.2	Recommendations	78

REFERENCES.....80

LIST OF TABLES

	Page
Table 4.1 Digitized 2D ERI ρ_A values at each MT station	48
Table 4.2 Digitized 2D ERI ρ_T values at each MT station.....	52
Table 4.3 RMS error comparison between ρ_A shift and ρ_T shift at every MT station.....	67
Table 4.4 Digitized resistivity values at intersection station of 2D inversion profiles	75

LIST OF FIGURES

	Page
Figure 2.1	Sources of EM field; (a) lightning activity and (b) solar wind interaction (Timothy & Nwankwo Levi, 2020) 7
Figure 2.2	The EM fields distribution including the dead band (Chave, 2017)... 8
Figure 2.3	Illustration of a 1D Earth (Martí, 2014)..... 11
Figure 2.4	Illustration of a 2D Earth (Martí, 2014)..... 12
Figure 2.5	Two independent modes in 2D Earth (Wang et al., 2021)..... 13
Figure 2.6	Illustration of a 3D earth (Martí, 2014)..... 14
Figure 2.7	Example of MT signal that is deviated from actual resistivity curve due to static shift. The curves have the same pattern but have different resistivity values (Ruiz-Aguilar et al., 2020) 15
Figure 2.8	Voltage-distance graph over a uniform half-space (Jiracek, 1990) ... 16
Figure 2.9	Voltage measurement over 5D length (Jiracek, 1990)..... 16
Figure 2.10	Primary and secondary electric fields encounter different mediums; a) conductive and b) resistive anomaly. Total current flow in the subsurface with the presence of; c) conductive and d) resistive anomaly (Jiracek, 1990)..... 18
Figure 2.11	Electrical field distributions in a topographic survey area (Jiracek, 1990) 19
Figure 2.12	TEM data acquisition layout (Chalikakis et al., 2004) 20
Figure 2.13	Comparison of data obtained from TEM and MT surveys where galvanic distortion presents in MT data (Hacıoğlu et al., 2018)..... 21
Figure 2.14	An example of MT data under telluric distortion as compared to TEM (Mwakirani et al., 2017) 22
Figure 2.15	VES electrodes arrangement (Malanda et al., 2018) 23

Figure 2.16	Subsurface model derived from VES, MT and joint inversion (VES + MT) as compared to borehole data (Harinarayana, 1999)....	25
Figure 2.17	Comparison between results from; (a) VES and (b) 2D ERI (AL-Menshed & Thabit, 2018).....	26
Figure 2.18	Different resistivity models obtained from; a) 2D ERI and b) TEM (Ardali et al., 2018).....	28
Figure 3.1	Study work flowchart.....	32
Figure 3.2	Geology map of Lahad Datu area (modified from Tate 2002).....	33
Figure 3.3	ABEM instrument for 2D ERI data acquisition.....	34
Figure 3.4	2D ERI survey lines and MT stations location.....	35
Figure 3.5	MT data acquisition equipment.....	37
Figure 3.6	Non-polarized electrodes; (a) in the casing and (b) buried in the ground.....	38
Figure 3.7	Setting up the induction coil for data acquisition; a) aligned and levelled, and b) buried.....	39
Figure 3.8	MT instrument layout during data acquisition.....	39
Figure 3.9	Static shift correction using ZondMT2D software where (a) is the apparent resistivity graph, (b) is digitized ρ_T (c) is phase graph and (d) is corrected resistivity curve.....	42
Figure 4.1	2D apparent resistivity profile for line NS1 and the location of MT01 station.....	45
Figure 4.2	2D apparent resistivity profile for line NS2 and the location of MT03 station.....	45
Figure 4.3	2D apparent resistivity profile for line NS3 and the location of MT04 station.....	46
Figure 4.4	2D apparent resistivity profile for line NS4 and the location of MT05 station.....	46
Figure 4.5	2D apparent resistivity profile for line WE1 and the location of MT06 station.....	46

Figure 4.6	2D apparent resistivity profile for line WE2 and the location of MT07 station.....	47
Figure 4.7	2D apparent resistivity profile for line WE3 and the location of MT02 station.....	47
Figure 4.8	2D apparent resistivity profile for line WE4 and the location of MT08 station.....	47
Figure 4.9	2D inversion model for line NS1 and the location of MT01 station .	48
Figure 4.10	2D inversion model for line NS2 and the location of MT03 station .	49
Figure 4.11	2D inversion model for line NS3 and the location of MT04 station .	49
Figure 4.12	2D inversion model for line NS4 and the location of MT05 station .	49
Figure 4.13	2D inversion model for line WE1 and the location of MT06 station	50
Figure 4.14	2D inversion model for line WE2 and the location of MT07 station	50
Figure 4.15	2D inversion model for line WE3 and the location of MT02 station	50
Figure 4.16	2D inversion model for line WE4 and the location of MT08 station	51
Figure 4.17	Compilation of 2D resistivity inversion models in the study area.....	51
Figure 4.18	MT data for N-S profile, a) apparent resistivity profile, b) apparent resistivity against period, c) phase profile and d) phase against period	53
Figure 4.19	MT data for W-E profile, a) apparent resistivity profile, b) apparent resistivity against period, c) phase profile and d) phase against period	53
Figure 4.20	Skewness value for each station displayed in profiles; (a) N-S and (b) W-E	54
Figure 4.21	Strike direction for N-S profile, (a) before and (b) after rotation	55
Figure 4.22	Strike direction for W-E profile, (a) before and (b) after rotation.....	56
Figure 4.23	Static shift correction using apparent resistivity data for MT01 station where; (a) the phase graph, (b) digitized ρ_A graph (c) apparent resistivity graph and (d) corrected resistivity curve after removing static shift.....	57

Figure 4.24	Static shift correction using apparent resistivity data for MT02 station where; (a) the phase graph, (b) digitized ρ_A graph (c) apparent resistivity graph and (d) corrected resistivity curve after removing static shift.....	58
Figure 4.25	Static shift correction using apparent resistivity data for MT03 station where; (a) the phase graph, (b) digitized ρ_A graph (c) apparent resistivity graph and (d) corrected resistivity curve after removing static shift.....	58
Figure 4.26	Static shift correction using apparent resistivity data for MT04 station where; (a) the phase graph, (b) digitized ρ_A graph (c) apparent resistivity graph and (d) corrected resistivity curve after removing static shift.....	59
Figure 4.27	Static shift correction using apparent resistivity data for MT05 station where; (a) the phase graph, (b) digitized ρ_A graph (c) apparent resistivity graph and (d) corrected resistivity curve after removing static shift.....	59
Figure 4.28	Static shift correction using apparent resistivity data for MT06 station where; (a) the phase graph, (b) digitized ρ_A graph (c) apparent resistivity graph and (d) corrected resistivity curve after removing static shift.....	60
Figure 4.29	Static shift correction using apparent resistivity data for MT07 station where; (a) the phase graph, (b) digitized ρ_A graph (c) apparent resistivity graph and (d) corrected resistivity curve after removing static shift.....	60
Figure 4.30	Static shift correction using apparent resistivity data for MT08 station where; (a) the phase graph, (b) digitized ρ_A graph (c) apparent resistivity graph and (d) corrected resistivity curve after removing static shift.....	61
Figure 4.31	Static shift correction using apparent resistivity data for MT09 station where; (a) the phase graph, (b) digitized ρ_A graph (c) apparent resistivity graph and (d) corrected resistivity curve after removing static shift.....	61

Figure 4.32	Static shift correction using true resistivity data for MT01 station where; (a) the phase graph, (b) digitized ρ_T graph (c) apparent resistivity graph and (d) corrected resistivity curve after removing static shift	62
Figure 4.33	Static shift correction using true resistivity data for MT02 station where; (a) the phase graph, (b) digitized ρ_T graph (c) apparent resistivity graph and (d) corrected resistivity curve after removing static shift	63
Figure 4.34	Static shift correction using true resistivity data for MT03 station where; (a) the phase graph, (b) digitized ρ_T graph (c) apparent resistivity graph and (d) corrected resistivity curve after removing static shift	63
Figure 4.35	Static shift correction using true resistivity data for MT04 station where; (a) the phase graph, (b) digitized ρ_T graph (c) apparent resistivity graph and (d) corrected resistivity curve after removing static shift	64
Figure 4.36	Static shift correction using true resistivity data for MT05 station where; (a) the phase graph, (b) digitized ρ_T graph (c) apparent resistivity graph and (d) corrected resistivity curve after removing static shift	64
Figure 4.37	Static shift correction using true resistivity data for MT06 station where; (a) the phase graph, (b) digitized ρ_T graph (c) apparent resistivity graph and (d) corrected resistivity curve after removing static shift	65
Figure 4.38	Static shift correction using true resistivity data for MT07 station where; (a) the phase graph, (b) digitized ρ_T graph (c) apparent resistivity graph and (d) corrected resistivity curve after removing static shift	65
Figure 4.39	Static shift correction using true resistivity data for MT08 station where; (a) the phase graph, (b) digitized ρ_T graph (c) apparent resistivity graph and (d) corrected resistivity curve after removing static shift	66

Figure 4.40	Static shift correction using true resistivity data for MT09 station where; (a) the phase graph, (b) digitized ρ_T graph (c) apparent resistivity graph and (d) corrected resistivity curve after removing static shift	66
Figure 4.41	2D N-S resistivity profile for no shift model	70
Figure 4.42	2D W-E resistivity profile for no shift model	70
Figure 4.43	2D N-S resistivity profile for ρ_A shift model	70
Figure 4.44	2D W-E resistivity profile for ρ_A shift model	71
Figure 4.45	2D N-S resistivity profile for ρ_T shift model	71
Figure 4.46	2D W-E resistivity profile for ρ_T shift model	71
Figure 4.47	3D fence diagram for no shift model as viewed from southeast direction	72
Figure 4.48	3D fence diagram for no shift model as viewed from southwest direction	72
Figure 4.49	3D fence diagram for ρ_A shift model as viewed from southeast direction	73
Figure 4.50	3D fence diagram for ρ_A shift model as viewed from southwest direction	73
Figure 4.51	3D fence diagram for ρ_T shift model as viewed from southeast direction	74
Figure 4.52	3D fence diagram for ρ_T shift model as viewed from southwest direction	74

LIST OF SYMBOLS

a	Electrode spacing
E	Electric field
H	Magnetic field
Hz	Hertz
I	Current
Im	Imaginary component
km	Kilometre
m	metre
Ma	Million years ago
Re	Real component
s	Second
T	Period
V	Voltage/Potential
Z	Impedance
ω	Angular frequency
ρ_A	Apparent resistivity
σ	Conductivity
ρ_T	True resistivity
Φ	Phase
μ	Magnetic permeability
δ	Skin depth
ΔV	Potential difference
f	Frequency
Ωm	Ohm.meter
β	Skewness
%	Percent/percentage

LIST OF ABBREVIATIONS

1D	One dimensional
2D	Two dimensional
3D	Three dimensional
DC	Direct current
EM	Electromagnetic
ERI	Electrical resistivity imaging
GPS	Global positioning system
MT	Magnetotellurics
N-S	North-South
RMS	Root mean square
TEM	Transient electromagnetic
TE	Transverse electric
TM	Transverse magnetic
VES	Vertical Electrical Sounding
W-E	West-East

**PENDEKATAN BARU DALAM PEMBETULAN ANJAKAN STATIK UNTUK
DATA MAGNETOTELLURIK MENGGUNAKAN PENGIMEJAN
KEBERINTANGAN ELEKTRIK 2D**

ABSTRAK

Kaedah Magnetotelurik (MT) menggunakan aktiviti kilat dan interaksi angin solar sebagai sumber elektromagnet dalam mengukur taburan keberintangan hingga kedalaman yang sangat jauh. Anjakan statik ialah sebuah masalah lazim dalam MT yang mana data MT sebenar teranjak lebih tinggi atau lebih rendah dalam skala log tetapi masih mengekalkan lengkungan keberintangan ketara (ρ_A) yang sama. Ia timbul daripada tiga faktor utama iaitu herotan voltan, herotan arus dan kesan topografi. Setakat ini, anjakan statik MT diperbetulkan menggunakan data pembunyian elektrik tegak (VES) dan elektromagnet fana (TEM), yang memberikan data keberintangan ketara dalam 1D yang tidak menggambarkan material subpermukaan dengan tepat. Sebaliknya, pengimejan keberintangan elektrik 2D (2D ERI) membekalkan data pada arah mengufuk dan menegak. Oleh itu, ia menghasilkan gambaran bawah tanah lebih baik dengan kepekaan lebih tinggi terhadap ketakhomogenan. Tambahan pula, keberintangan sebenar (ρ_T) yang diperoleh selepas songsangan memberikan gambaran bumi yang lebih baik berbanding ρ_A . Oleh itu, kajian ini membangunkan pembetulan anjakan statik yang baharu menggunakan data keberintangan sebenar 2D ERI. Kajian ini telah dijalankan pada tahun 2020 yang mana sembilan stesen MT telah dijalankan di Lahad Datu, Sabah. Garis-garis tinjauan 2D ERI telah dijalankan merentangi setiap stesen MT untuk mendapatkan model keberintangan terbaik dan mendapatkan nilai-nilai ρ_A dan ρ_T di bawah stesen MT sebagai dua kumpulan data untuk pembetulan anjakan statik. Data keberintangan daripada 2D ERI telah digunakan untuk

mengekang songsangan fasa MT untuk mendapatkan respons sebenar MT bagi setiap stesen MT. Lengkung keberintangan daripada tinjauan MT kemudiannya dianjurkan ke respond sebenar untuk mencapai aras sebenar data keberintangan. Hasil-hasil yang diperoleh daripada anjakan ρ_A dan ρ_T telah mengeluarkan nilai RMS masing-masing iaitu <11.3 dan <8.1 . Nilai RMS yang lebih rendah menunjukkan bahawa anjakan ρ_T adalah lebih berkesan dalam membuang kesan anjakan statik. Hasil tersebut kemudiannya digunakan sebagai input untuk proses songsangan MT. Songsangan MT telah dijalankan terhadap tiga data: tanpa pembetulan anjakan statik, pembetulan menggunakan ρ_A dan pembetulan menggunakan ρ_T untuk menjana profil 2D dan rajah pagar 3D dalam menentukan model terbaik yang mewakili subpermukaan tanah. Secara kualitatif, model tanpa pembetulan anjakan statik menghasilkan nilai-nilai keberintangan yang tidak logik sementara model-model lain boleh diterima pakai. Daripada pemerhatian rajah-rajah 3D, model anjakan ρ_A menunjukkan taburan keberintangan yang tidak padan pada persilangan antara profil Utara-Selatan (N-S) dan Barat-Timur (W-E), sementara model anjakan ρ_T menunjukkan hasil yang sepadan. Oleh itu, model anjakan ρ_T mengungguli analisis kualitatif. Analisis kuantitatif terhadap tiga model tersebut juga dijalankan dengan membandingkan peratusan perbezaan nilai keberintangan di persilangan antara profil N-S dan W-E. Model anjakan ρ_T mempunyai peratusan perbezaan paling rendah ($<38\%$) berbanding dua model yang lain. Ini menunjukkan bahawa prestasi pendekatan baharu pembetulan anjakan statik MT menggunakan ρ_T mengatasi kaedah konvensional dan andal untuk kegunaan masa hadapan.

**NOVEL APPROACH IN STATIC SHIFT CORRECTION FOR
MAGNETOTELLURICS DATA USING 2D ELECTRICAL RESISTIVITY
IMAGING**

ABSTRACT

Magnetotellurics (MT) method utilizes lightning activities and solar wind interactions as electromagnetic sources in measuring resistivity distribution to great depths. Static shift is a common problem in MT where actual MT data is shifted higher or lower in logarithmic scale but maintains the same apparent resistivity (ρ_A) curve. It arises from voltage distortion, current distortion and topography effect. Currently, MT static shift is corrected using vertical electrical sounding (VES) and transient electromagnetic (TEM) data, which give ρ_A data in 1D that does not depict subsurface materials precisely. In contrast, 2D electrical resistivity imaging (2D ERI) provides data in lateral and vertical directions; therefore, better images the ground with higher sensitivity to inhomogeneity. Additionally, true resistivity (ρ_T) obtained after inversion provides a better representation of the Earth than ρ_A . Therefore, this study develops a new static shift correction using 2D ERI ρ_T data. The study was carried out in 2020 where nine MT stations were conducted in Lahad Datu, Sabah. 2D ERI lines were conducted across MT stations to obtain the best resistivity model and extract ρ_A and ρ_T values beneath MT stations as two data groups for static shift correction. Resistivity data from 2D ERI was employed to constrain MT phase inversion to obtain the actual MT response for every MT station. Resistivity curve from MT survey was then shifted to the actual response to achieve its true resistivity level. The results obtained from ρ_A and ρ_T shifts yielded RMS values of <11.3 and <8.1 respectively. The lower RMS values indicate that the ρ_T shift is more effective

in removing static shift effect. The results were then used as input for MT inversion process. MT inversion was conducted on three data: without static shift correction, correction using ρ_A and correction using ρ_T to generate 2D profiles and 3D fence diagrams in determining the best model to represent the subsurface. Qualitatively, model without static shift correction yielded illogical resistivity values while the other models were acceptable. From 3D diagrams observation, ρ_A shift model shows mismatched resistivity distribution at the intersection between North-South (N-S) and West-East (W-E) profiles, while ρ_T shift model shows well-matched results, therefore, outperforms in qualitatively analysis. Quantitative analysis on the three models by comparing percentage difference of resistivity values at profiles intersection was also conducted. The ρ_T shift model has the lowest percentage difference (<38%) than the others. This showcases that the performance of novel MT static shift correction using ρ_T surpasses conventional method and is reliable for future usage.

CHAPTER 1

INTRODUCTION

1.1 Background

Magnetotellurics (MT) is a passive geophysical method that measures resistivity distribution of a subsurface using natural electromagnetic (EM) sources such as lightning activities and solar wind interaction. The biggest advantage of this method is its penetration depth that reaches down to crust and upper mantle (Käufel et al., 2020; Yu et al., 2020). Thus, MT method has been widely applied in various applications such as geothermal (Corbo-Camargo et al., 2020; Samrock et al., 2018; Yadav et al., 2020), fault system (Díaz et al., 2020; Pearce et al., 2020), tectonic study (Azeez et al., 2017; Tzanis et al., 2020) and petroleum exploration (Miri et al., 2021; Palshin et al., 2020).

By employing MT method, inductive response of the Earth allows scientists to obtain information on the electrical resistivity of the subsurface and determine the dimensionality of the measured body. However, despite the method's advantages, MT is affected by galvanic distortion generated by small scale inhomogeneity located at near-surface (Santilano et al., 2018; Tang et al., 2018). This drawback is called static shift which primarily affects measured electric field and causes distortion of field response (Coppo et al., 2014). This leads to the measured MT apparent resistivity values to be multiplied by a scale factor, therefore, the values become inaccurate if left uncorrected (Karlsdóttir et al., 2020).

Traditionally, the static shift problem is tackled by applying curve shift estimation (Jiracek, 1990). The idea is to employ other geophysical methods such as transient electromagnetic (TEM) and vertical electrical sounding (VES) to recover near-surface resistivity as complementary data to MT (Hacıoğlu et al., 2018; Mwakirani et al., 2017; Wazny et al., 2018). For this purpose, the methods are usually conducted on MT location to generate 1-dimension (1D) apparent resistivity data at shallow depth. They were utilized as reference to recover MT apparent resistivity curve.

1.2 Problem statement

The most common geophysical methods reported for MT static shift correction are VES and TEM. However, TEM equipment is not always readily available, especially in Malaysia. Meanwhile, 2-dimensional electrical resistivity imaging (2D ERI) is widely employed in various fields for subsurface study such as geophysics and engineering. Therefore, implementation of 2D ERI for MT static shift correction will allow more practitioners to utilize their existing instrument in MT study.

VES and TEM methods only provide users with apparent resistivity data. The data represents average resistivity values of different earth layers at measured point which does not exactly reflect the earth material (Loke, 2004). Their data are also of 1D nature in a vertical direction under a single station. In contrast, 2D ERI provides true resistivity data that represents the actual resistivity values of the subsurface through inversion process. Lateral and vertical data coverage of 2D ERI method produces a more accurate resistivity model that best represents the Earth. Hypothetically, the new approach will provide more accurate outputs.

1.3 Research objectives

This study applied MT and 2D ERI methods with the objectives of;

- i. To construct static shift correction using 2D ERI apparent and true resistivity values.
- ii. To analyse MT static shift correction using apparent and true resistivity values.
- iii. To determine the best MT inversion model from three different approaches: apparent resistivity, true resistivity and no shift.

1.4 Scope of study

This study focuses on static shift correction of MT data using 2D ERI method. The survey was conducted in Lahad Datu, Sabah with a total of nine MT stations and eight 2D ERI survey lines. Each resistivity survey line crosses MT station for data correlation. MT data were processed using KMS-200 and ZondMT2D software to produce apparent resistivity and phase graphs. Two types of data were extracted from 2D ERI survey which are apparent resistivity and true resistivity, which were used for the static shift correction individually.

Both approaches were compared to determine the effectiveness of each method in removing the static shift effect. This study also conducted an inversion process on three different MT data types: without static shift correction, correction using apparent resistivity and correction using true resistivity. Models generated from the inversion were visualised in 2D profiles and 3D fence diagrams to analyse and determine the

best performance. Further qualitative analysis was conducted to complement the finding and conclude the best approach to solve MT static shift problem.

1.5 Novelty

Previous studies have shown the application of TEM and VES for MT static shift correction in various places with different geological formations. These methods were also applied to remove the effect using apparent resistivity values. This study proposes a new method in resolving MT static shift problem using 2D ERI which has never been done. This novel approach also utilizes true resistivity values as input, which differs from conventional approaches that employs apparent resistivity values. If this study is proven successful, more researchers are able to conduct MT static shift correction by utilizing 2D ERI method as the instrument is more widely available especially in Malaysia. Moreover, 2D ERI may increase the accuracy of MT static shift correction as it has greater capability in mapping the subsurface.

1.6 Thesis layout

This thesis is divided into five chapters. Chapter 2 introduces basic theory of the MT method which includes signal sources, MT transfer function and types of dimensionalities. An insight of static shift effects is described in detail together with common methods used to overcome the problem. Chapter 3 provides information on methods, instruments, layout and survey details to obtain field data. The procedures to conduct static shift correction from MT and 2D ERI data are explained thoroughly. In chapter 4, an overview of data extraction from 2D ERI is explained and is followed by

MT data processing. Detailed static shift correction using apparent and true resistivity data are disclosed, followed by inversion of three different types of MT data and further analyses. Finally, the summary and conclusion of this study is covered in Chapter 5.

CHAPTER 2

LITERATURE REVIEW

2.1 Introduction

This chapter starts with a brief introduction on magnetotellurics (MT). This method utilizes natural varying electromagnetic (EM) sources as input to measure earth resistivity from shallow to deep subsurface. From electric and magnetic fields responses measured on the ground, this section defines the calculations for impedance tensor, apparent resistivity, phase angle and penetration depth. Different types of dimensionalities that a ground might possibly have, prior to choose the appropriate inversion/modelling are also discussed here.

This is followed by a discussion on static shift problem that commonly occurs in MT survey. The issue, possible causes and the way to overcome are deliberated in detail as well as previous studies related to the topic. A review on 2D electrical resistivity imaging (2D ERI); basic concept, its capability to resolve different earth materials in the ground and comparison to conventional methods are also compiled in this chapter. Lastly, this chapter highlights the novelty of this study.

2.2 Electromagnetic (EM) sources

Magnetotellurics is a passive method that utilizes naturally occurring electromagnetic (EM) waves derived from lightning activities and solar wind interactions (Platz, 2018; Tank et al., 2018; Timothy & Nwankwo Levi, 2020).

Thunderstorm activities around the globe contribute to the EM signal in the period range shorter than 1 s, where the events mostly occur in tropical regions (Chen et al., 2021; Simpson & Bahr, 2005). The energy is sufficient to create EM signal to any location on the earth's surface as it can travel for long distances by propagating inside an insulating waveguide between conductive earth surface and ionosphere (Figure 2.1a).

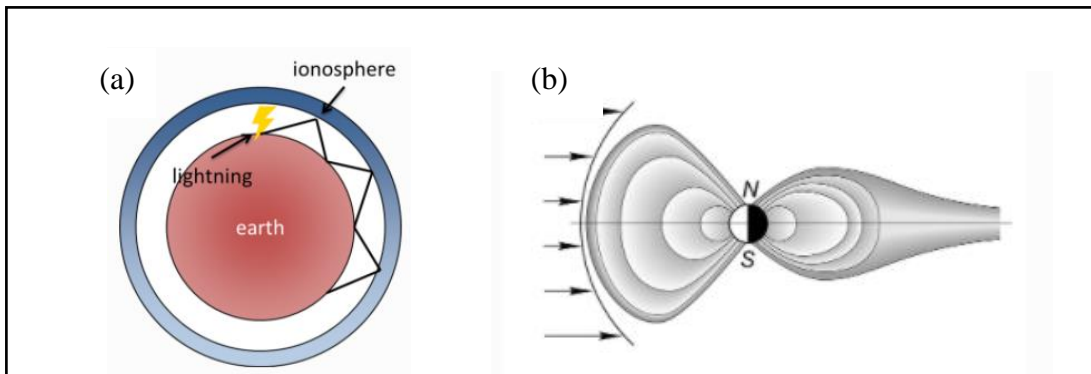


Figure 2.1: Sources of EM field; (a) lightning activity and (b) solar wind interaction (Timothy & Nwankwo Levi, 2020)

Interaction between solar wind (from the Sun) and Earth magnetic field generates EM fields in periods range of 1 s to 10^5 s as shown in Figure 2.1b (Abimanyu & Daud, 2021; Le et al., 2019). As the solar wind encounters the Earth's magnetic field, some energy pass through the layer and arrive at the highly conductive ionosphere. Further interactions between them generate EM field that propagates down towards the Earth surface (McPherron, 2005). Around period of 1 s, there is a narrow period range of 0.2 s to 2 s known as the dead band where EM field signal is at minimum amplitude (Chave, 2017; Martí, 2006). This is due to the low geomagnetic activity in that particular frequency (Smirnov et al., 2018). The distribution of high frequency, low frequency and dead band EM field signal is shown in Figure 2.2.

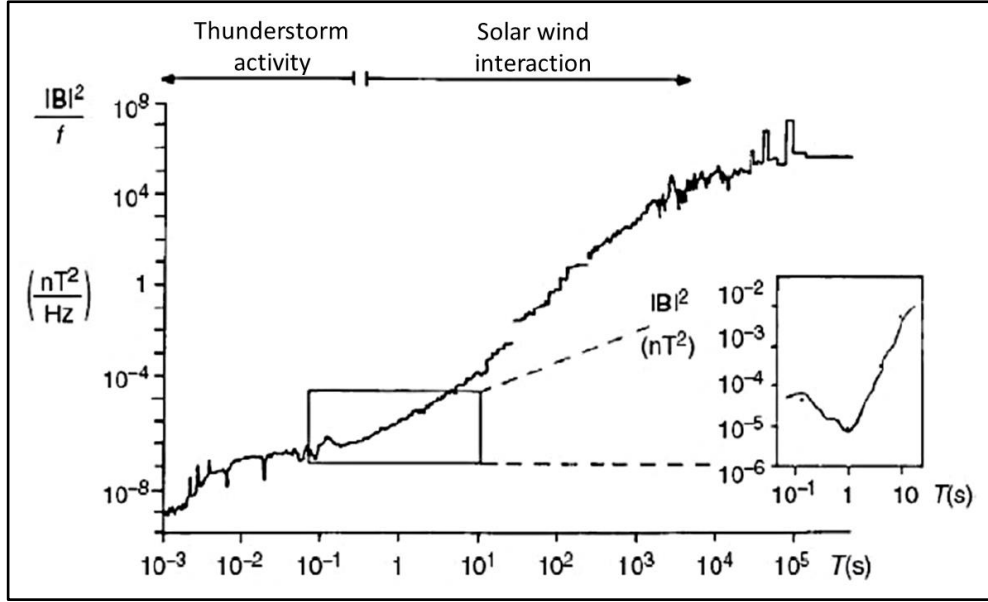


Figure 2.2: The EM fields distribution including the dead band (Chave, 2017).

2.3 Transfer function

An MT transfer function is a function that describes the relationship between measured electric and magnetic fields at specified frequencies that are solely dependent on the electrical properties of the Earth where EM fields propagate (Bonner & Schultz, 2017). Therefore, it directly portrays the conductivity/resistivity of underlying subsurface. The most common transfer function, and chosen for this study is impedance tensor (Bonner & Schultz, 2017; Palshin et al., 2020).

The impedance tensor is commonly denoted as \mathbf{Z} , which is a complex and frequency-dependent matrix that describes the ratio between orthogonal horizontal EM fields; electric (E_x , E_y) and magnetic (H_x , H_y) (Grayver et al., 2019; Varılsüha, 2020). Equations 2.1 and 2.2 show the initial relation between electric and magnetic fields which can be expanded into their respective components,

$$E = ZH \quad (2.1)$$

$$\begin{pmatrix} E_x \\ E_y \end{pmatrix} = \begin{pmatrix} Z_{xx} & Z_{xy} \\ Z_{yx} & Z_{yy} \end{pmatrix} \begin{pmatrix} H_x \\ H_y \end{pmatrix} \quad (2.2)$$

Where;

E_x	=	electric field in x-direction
E_y	=	electric field in y-direction
H_x	=	magnetic field in x-direction
H_y	=	magnetic field in y-direction
Z_{xx}	=	ratio of E_x/H_x
Z_{xy}	=	ratio of E_x/H_y
Z_{yx}	=	ratio of E_y/H_x
Z_{yy}	=	ratio of E_y/H_y

Impedance tensor is closely related to apparent resistivity, ρ_a and impedance phase, Φ . The variable ρ_a is defined by the resistivity value of a uniform half-space measured at a particular frequency (Bowles-Martinez, 2019; Marsenić, 2020), while the impedance phase is the phase delay between electric and magnetic fields (Unsworth, 2007). The relationships are given by Equations 2.3 and 2.4.

$$\rho_a = \frac{1}{\mu\omega} |Z|^2 \quad (2.3)$$

$$\Phi = \tan^{-1} \frac{Im Z}{Re Z} \quad (2.4)$$

Where;

ρ_a	=	apparent resistivity
μ	=	magnetic permeability
ω	=	angular frequency
Z	=	impedance tensor
Φ	=	impedance phase
$Im Z$	=	imaginary component of Z
$Re Z$	=	real component of Z

The initial impedance phase is 45° for all frequencies as EM fields travel from air into the Earth and remain the same as long as they propagate in a homogeneous half-space (Thiel, 2008). However, in the real Earth, the value will vary with the underlying geological structure. An increase in phase angle value indicates that the

EM signal travels to a more conductive material while phase angle reduces as the fields travel to a more resistive material (Chen et al., 1996; Li et al., 2020b).

EM field propagates at different frequencies. Low frequency signal can penetrate deeper while high frequency is better in resolving shallow subsurface (Liang et al., 2020; Wei Li, 2020). As the waves travel from air to earth medium, the amplitude will reduce gradually. Distance from the ground surface at which the EM wave attenuates to 1/e (or 37 %) of its original amplitude is called skin depth (Equation 2.5), where it is often used as depth of investigation (Saputra & Widodo, 2017; Timothy & Nwankwo Levi, 2020).

$$\delta = 500\sqrt{T\rho_a} \quad (2.5)$$

Where;

δ = skin depth
 T = period
 ρ_a = apparent resistivity

2.4 Dimensionality

It is vital to recognize the dimensionality of a study area prior to modelling and analysis steps (Gao et al., 2018). Generally, conductivity/resistivity distribution of the subsurface is classified into three geoelectric dimensionalities: 1-dimension (1D), 2-dimension (2D) and 3-dimension (3D). Each dimensionality represents different soil/rock characteristics, impedance tensor complexity and MT assumptions that cannot be violated (Bowles-Martinez, 2019). Choosing a different dimensionality analysis for a set of data or totally ignoring the dimensionality analysis will lead to

inaccuracy of the Earth model and misleading interpretations (Beka et al., 2017; Ledo, 2005; Ledo et al., 2002).

2.4.1 1D Earth

1D Earth refers to horizontal layered-ground or stratified geological formation such as delta and basin (Figure 2.3). The conductivity is uniform in the lateral direction but changes with depth (Martí, 2014). Due to its condition, the transfer function for this type of model is independent of any measurement orientation, thus, no rotation of the dataset is needed.

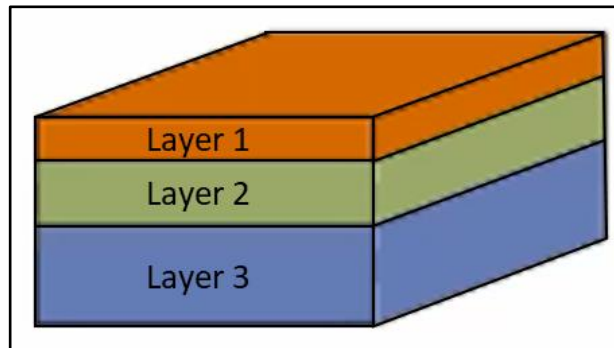


Figure 2.3: Illustration of a 1D Earth (Martí, 2014)

The nature of this geological condition permits the simplification of original impedance tensor components from Equation 2.2. Parallel EM in the same direction in relation to diagonal components (Z_{xx} and Z_{yy}) is equals to zero. The ratio of E/H is the same in all directions and off-diagonal components (Z_{xy} and Z_{yx}) have the same amplitude but in opposite direction (Martí, 2014). Hence, the impedance tensor, Z component can be derived to become Equation 2.6.

$$Z = \begin{pmatrix} 0 & Z_{xy} \\ -Z_{xy} & 0 \end{pmatrix} \quad (2.6)$$

2.4.2 2D Earth

A 2D geological structure is represented by varying conductivity with depth in a single horizontal direction, while the other direction has an infinite structure with constant conductivity as shown in Figure 2.4 (Maithya & Fujimitsu, 2019). This feature typically portrays the existence of fault. The direction along the fault is called the geoelectric strike which provides uniform conductivity, while the direction perpendicular to it exhibits different conductivity values.

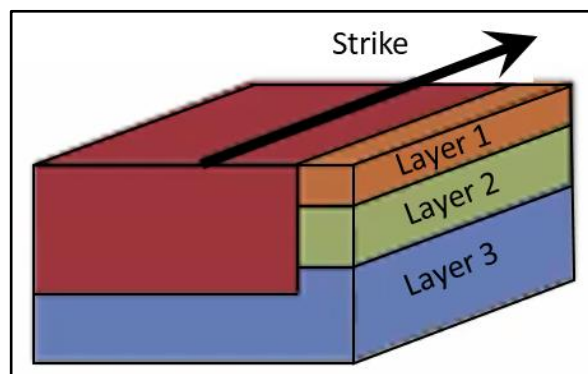


Figure 2.4: Illustration of a 2D Earth (Martí, 2014)

In an ideal 2D case, electric and magnetic fields are perpendicular to each other. When an electric field is parallel to the strike (E_x), this induces magnetic field in the plane perpendicular to the strike (H_y and H_z), while magnetic field perpendicular to the strike (H_x) induces electrical field plane perpendicular to the strike (E_y and E_z) as shown in Figure 2.5 (Berdichevsky & Dmitriev, 2008). Hence, they can be decoupled into two independent modes: transverse electric (TE) and transverse magnetic (TM). TE or E-polarization mode describes current flow along the strike while TM or B-polarization mode indicates current flow across the strike (Corseri et al., 2017; Mohan et al., 2017; Wang et al., 2021). Diagonal elements remain zero, while off-diagonal elements, Z_{xy} and Z_{yx} represent the two modes: TE and TM respectively (Corseri et al.,

2017; Wang et al., 2021). Thus, the impedance tensor for the 2D Earth can be simplified to Equation 2.7.

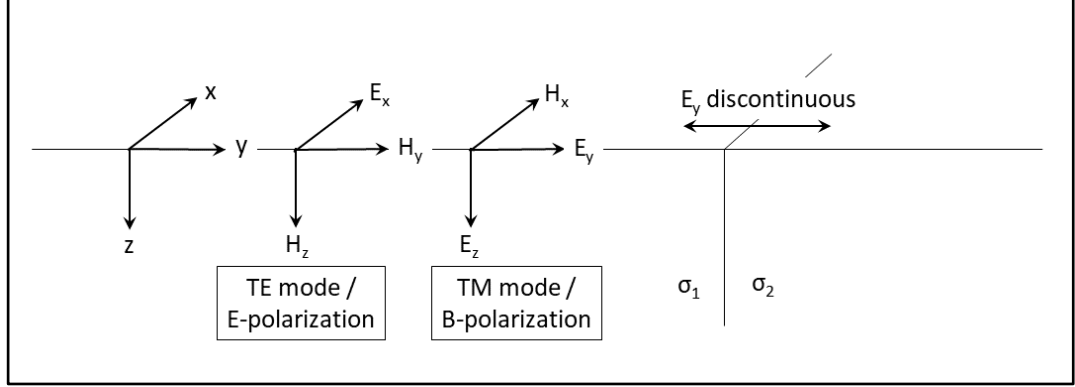


Figure 2.5: Two independent modes in 2D Earth (Wang et al., 2021).

$$Z = \begin{pmatrix} 0 & Z_{xy} \\ Z_{yx} & 0 \end{pmatrix} \quad (2.7)$$

2.4.3 3D Earth

The 3D Earth is the most general geological structure where conductivity varies in vertical and both horizontal directions as shown in Equation 2.8 and Figure 2.6. Due to its complex formation, any rotation of the dataset is invalid and cannot be decoupled into two different modes as 2D Earth. Hence, 3D Earth takes the full form of impedance tensor (Bedrosian & Love, 2015; Newman et al., 2015).

$$Z = \begin{pmatrix} Z_{xx} & Z_{xy} \\ Z_{yx} & Z_{yy} \end{pmatrix} \quad (2.8)$$

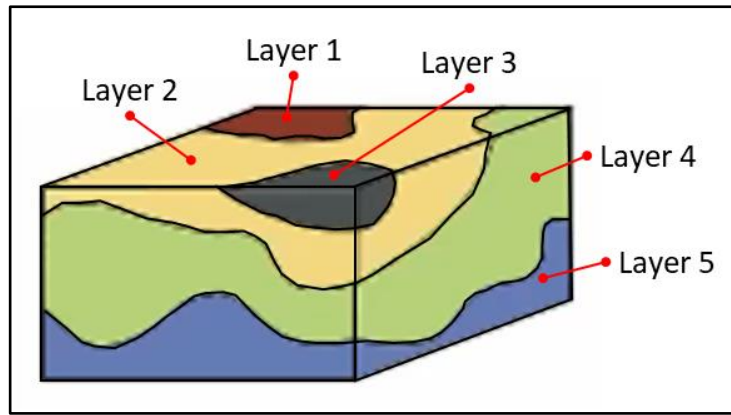


Figure 2.6: Illustration of a 3D earth (Martí, 2014)

2.5 Static shift

In practice, measured electrical field data in MT survey is often inaccurate due to noises (galvanic distortion) from near surface structures. This galvanic distortion is called static shift which induces a constant shift of the measured data in a logarithmic scale (Santilano et al., 2018; Tang et al., 2018). However, the effect is only afflicted to the electrical field data as the noise existed as the unwanted electrical field that interferes with the true signal. A resistivity curve under the static shift effect will retain the correct curve/pattern as they are frequency and phase independent (Luan et al., 2018; Tournier et al., 2007). However, the resistivity values obtained from MT survey are incorrect because they have deviated to higher or lower values (Figure 2.7a). Further modelling without appropriate correction will lead to inaccurate modelling and misinterpretation as shown in Figure 2.7b (Ruiz-Aguilar et al., 2020).

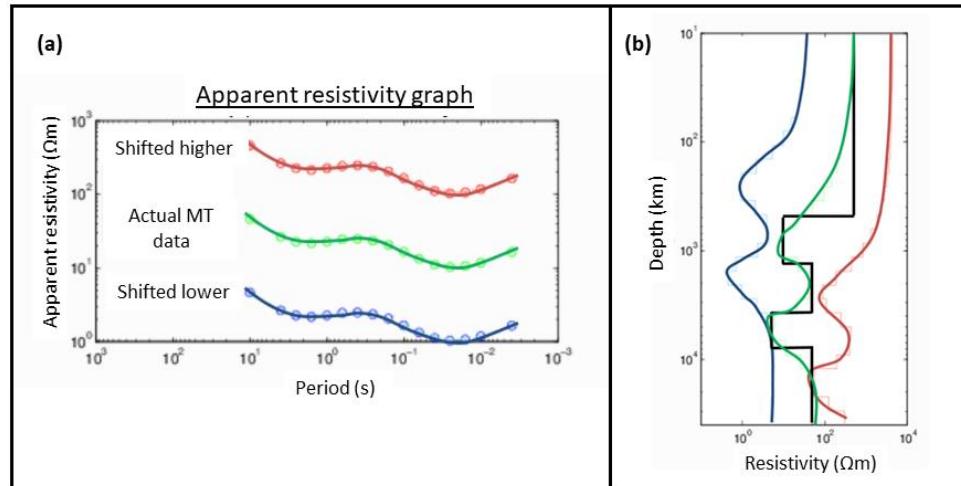


Figure 2.7: Example of MT signal that is deviated from actual resistivity curve due to static shift. The curves have the same pattern but have different resistivity values (Ruiz-Aguilar et al., 2020).

2.5.1 Static shift sources

Static shift arises from a few factors such as voltage distortion, current distortion and topography effects (Hersir & Flóvenz, 2013). Taking an example of a homogeneous half-space, an electric field is measured by calculating the potential difference between two poles over a finite distance. For instance, Figure 2.8 shows the average electric field can be defined by the gradient of the voltage-distance graph. A uniform conductive body allows a steady current flow and yields a slope with a constant gradient. Measurement at any point on the slope will generate a constant electric field value.

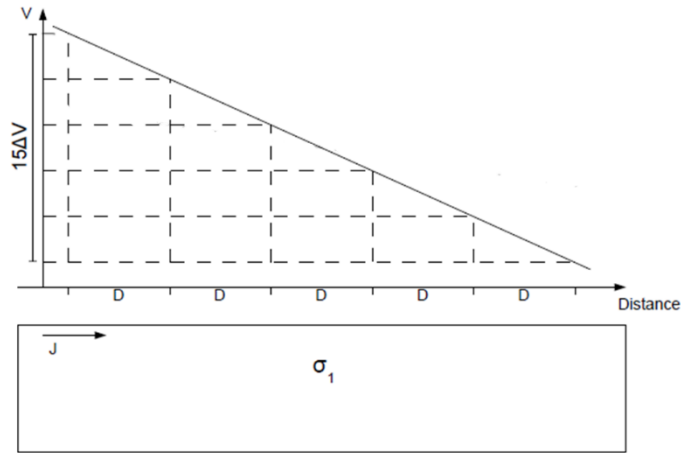


Figure 2.8: Voltage-distance graph over a uniform half-space (Jiracek, 1990).

Practically, common subsurface structure is hardly uniform and has varying conductivity with depths. Figure 2.9 showcases an example of inhomogeneous subsurface where two bodies with the conductivity of σ_1 sandwich a more conductive body with σ_2 . Note that the gradient of the slope is now inconstant. Magnetic field measurement at a given point on the graph will not be the same at all locations in the graph. Voltage measurement over $5D$ length will yield a lower potential value as compared to Figure 2.8 above (Wannamaker et al., 1996). Conversely, a higher potential value will be obtained if the anomaly is made of a higher resistivity value.

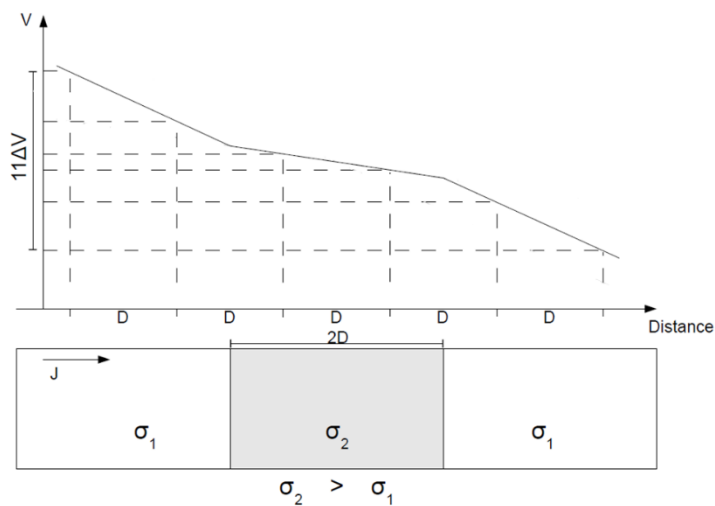


Figure 2.9: Voltage measurement over $5D$ length (Jiracek, 1990).

The static shift effect is severe especially on the shallow subsurface due to voltage is measured over a short distance (depth) to the surface. As the depth increases, the effect reduces as the width of the anomaly is now comparatively small to the total depth. Imprecise voltage values and electrical field measurement causes a shift in apparent resistivity from the true value.

Current flows in a half-space will be altered as they encounter a more conductive or resistive anomaly and the effect is proportional to conductivity of the body. Higher conductivity causes current to flow into the body (Figure 2.10a), while in contrast, it will deflect away from a more resistive body (Figure 2.10b). With the presence of primary electrical field across an anomaly, it will subsequently cause a charge build-up at the boundary between the body and its surrounding.

A resistive body causes the occurrence of positive charge build-up on the side that facing the primary wave and deflects the field away from it (Figure 2.10c). At the same time, a secondary field is induced within and around the anomaly which aligns with the main field. In the case of a conductive body, negative charges tend to accumulate on the side facing the primary field and generates a secondary field in the opposite direction of the primary field (Figure 2.10d). As the primary field flows into the anomaly, the change in electric field lines causes the inaccuracy of depth estimation (Figure 2.10). MT data is measured over the assumption of a uniform electric field in the subsurface to obtain depth. However, in the case of primary field lines are affected by the anomaly, it will be distorted from its original pattern. Note that the data is always measured following the electrical field lines, thus, the obtained data in a disturbed electrical field will be deeper for a conductive anomaly but shallower for a resistive anomaly (Berdichevsky & Dmitriev, 2008). This explains the static shift in MT data collection.

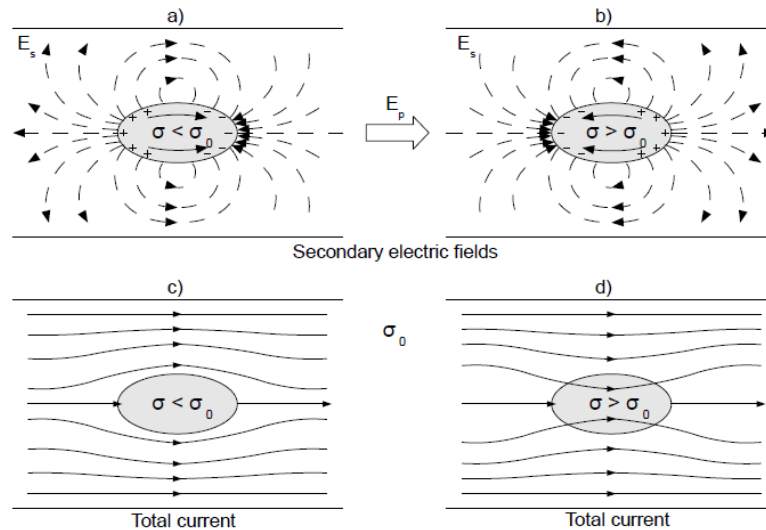


Figure 2.10: Primary and secondary electric fields encounter different mediums; a) conductive and b) resistive anomaly. Total current flow in the subsurface with the presence of; c) conductive and d) resistive anomaly (Jiracek, 1990).

Current behaves differently as they flow across topographic features such as hills and valleys as topography influences current density. As the primary electric field in the subsurface encounters a high elevation structure, negative charges align themselves with the hill slope that faces the primary field, while positive charges are at the back side (Figure 2.11). This creates a secondary field across the hill in the opposite direction, therefore, results in a lower electric field strength on the hill. The event also causes the secondary electric field to align with the primary field which adds up to produce higher electric field strength at the valley bottom (Kumar et al., 2018). A weak electrical signal might lead to inaccurate data, especially in depth estimation (Sarakorn & Vachirastienchai, 2018). However, one simply cannot draw a conclusion just to conduct an MT survey at the valley and avoid the hills as ground undulations are the observed clues of the Earth's complex formations such as faults, geothermal and ore deposits.

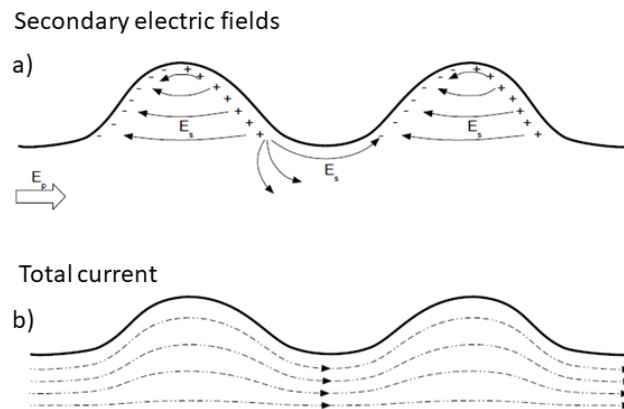


Figure 2.11: Electrical field distributions in a topographic survey area (Jiracek, 1990)

2.5.2 Static shift correction

Precautions must be taken whenever possible in order to obtain the most reliable data with minimum surrounding noise. Removing the static shift effect prior to inversion routine is vital as it could lead to erroneous results and misinterpretation of subsurface resistivity. Jiracek (1990) suggested one direct method to solve the problem by using curve shift estimation. The idea is to conduct another survey to ascertain the MT signal shifts from the original/expected curve (Farzamian et al., 2019; Moorkamp et al., 2020; Ruthsatz et al., 2018).

Two geophysical methods that are widely used as supplementary data for static shift corrections are transient electromagnetic (TEM) and vertical electrical sounding (VES). TEM is an active electromagnetic method that uses a controlled current source which is switched on and off alternately. Current is supplied into a wire loop on the ground to generate a vertical magnetic field into the subsurface (Figure 2.12). As the wave encounters different Earth materials, it induces eddy current to generate a secondary magnetic field that propagates back and is detected by a receiver loop on

the ground (Gonzales Amaya et al., 2018; Guo et al., 2019; Yu et al., 2017). The data is recorded over a certain period as the secondary field's amplitude decreases over time to illustrate the resistive property of the subsurface (Christiansen et al., 2006). This method provides the apparent resistivity data against time and effectively maps the subsurface up to 500 m (Cumming et al., 2010). Even though TEM has comparatively shallow penetration depth as compared to MT, this method is often used to compliment MT for static shift correction by resolving shallower part of the subsurface.

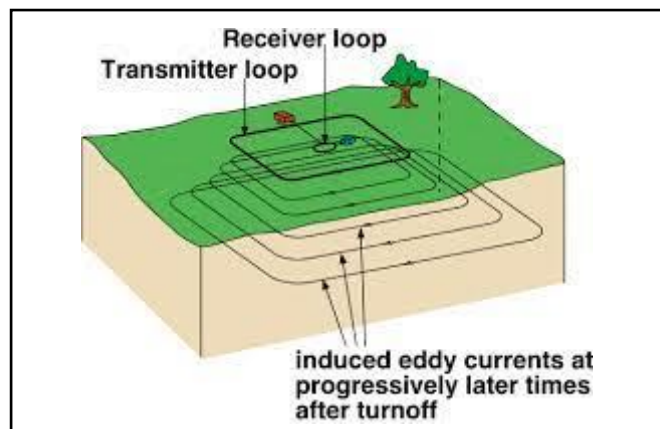


Figure 2.12: TEM data acquisition layout (Chalikakis et al., 2004)

While MT signal is much influenced by near-surface inhomogeneity, TEM is relatively unaffected by the small-scaled anomaly (Árnason et al., 2010; Ruiz-Aguilar et al., 2020; Sternberg et al., 1988). This is favourable for MT static shift correction as TEM only depends on the magnetic field and has no electrical contact with the ground, which is often related to galvanic distortion. For instance, six MT sites located at a volcanic area were predicted to be under the influence of static shift caused by topography and surface heterogeneity (Hacıoğlu et al., 2018). Apparent resistivity curves of off-diagonal elements are split at low periods which indicates a high probability of galvanic distortions. TEM survey was conducted on each MT station. The collected data was inversed and compared with MT resistivity curves (Figure 2.13). It was found that MT data are slightly higher and lower than of TEM along the

apparent resistivity curve, therefore, MT data curve was shifted accordingly. TEM is advantageous as a reference to improve MT data at shallow Earth.

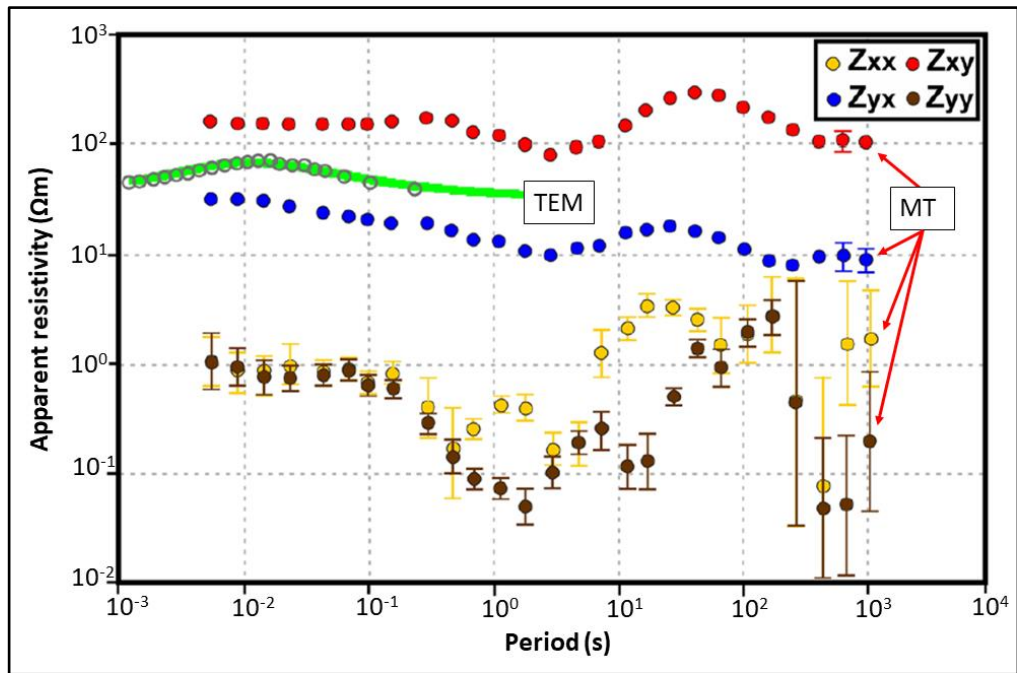


Figure 2.13: Comparison of data obtained from TEM and MT surveys where galvanic distortion presents in MT data (Hacıoğlu et al., 2018).

A study was conducted by integrating MT and TEM methods for static shift correction in Kenya (Mwakirani et al., 2017). Half of the MT stations are under telluric distortion (Figure 2.14). To overcome this, TEM survey was carried out on the MT stations. Data from both methods were joint inverted in 1D routine and the correct apparent resistivity values from MT were resolved. However, a distribution pattern of static shift factor in the study area is not uniform. This is because the galvanic effect is vary from one station to another which depends solely on the surface inhomogeneity (Santilano et al., 2018).

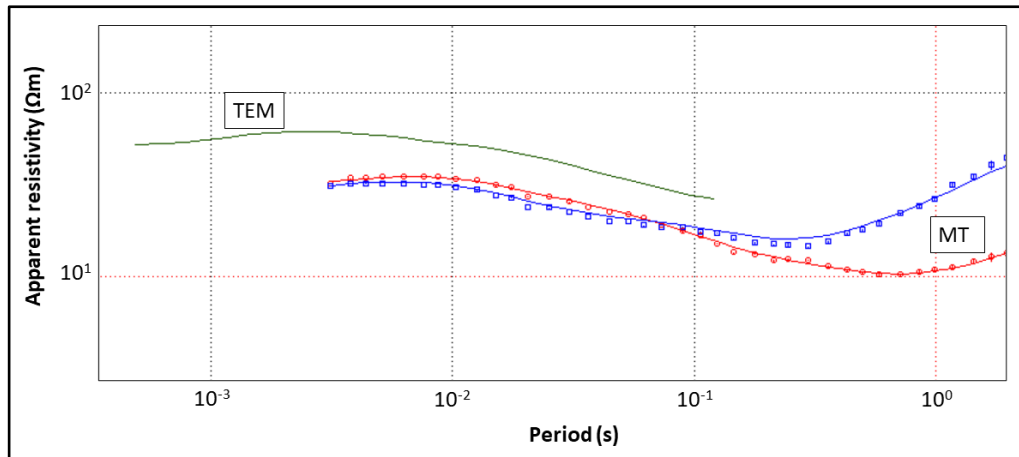


Figure 2.14: An example of MT data under telluric distortion as compared to TEM (Mwakirani et al., 2017).

Karlsdóttir et al., (2020) also used TEM at every MT station out to investigate the resistivity distribution in a geothermal area. Due to undulating topography, the raw MT data is much affected by the galvanic shift. Therefore, TEM was employed as a correction reference prior to modelling as this method is much less influenced by the topographic effect. The results obtained show that galvanic shift due to topography and surface inhomogeneity was successfully removed, thus, producing a reliable data for inversion. Same goes to another case study reported by Hersir et al. (2020) which implemented TEM data for static shift correction for over 100 MT stations. A combination of these methods is widely used in geothermal environments (Arnason, 2015). However, several rare cases have reported that the presence of thick resistive layer at the surface causes TEM to be less reliable in correcting galvanic distortion in MT (Cumming et al., 2010).

Another approach to obtain shallow subsurface apparent resistivity data for static correction is VES. This method implements the basic concept of four electrodes planted on the ground and aligned in a constant spacing (Figure 2.15). Current is injected using outer pair of electrodes to generate electric paths in the ground which creates equipotential line perpendicular to them. Another pair of electrodes is used to

measure the potential difference between the current electrodes where the measured value is used as input to obtain resistivity value.

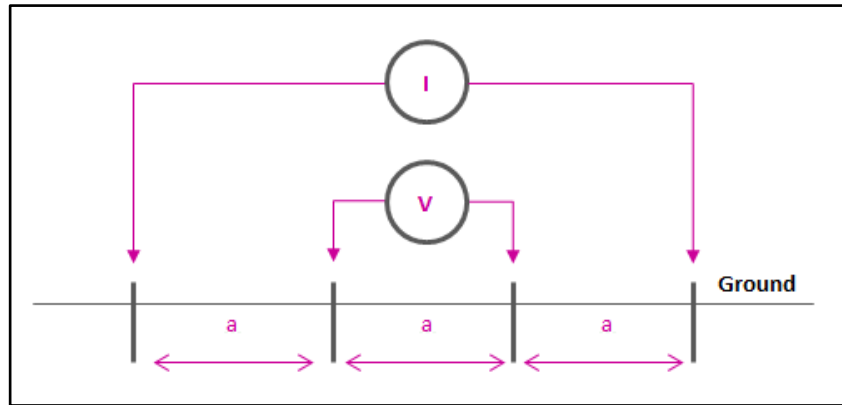


Figure 2.15: VES electrodes arrangement (Malanda et al., 2018)

Like TEM, measured MT data utilizes shallow resistivity data as reference for shifting the distorted data to a true level. Some literatures dispute the reliability of VES for galvanic distortion correction. The galvanic effect in MT commonly arises from electrical contact with the ground which is also conducted in VES data acquisition. Assuming that this statement is true, then VES is impractical for static shift correction as the method also has galvanic distortion. However, Romo et al., (1997) has proven that the near-surface boundary effect is negligible for VES as compared to MT due to the arrangement between source and receiver electrodes. Spitzer (2001) explained that the area between potential electrodes downward is called positive sensitivity region where measurement is taken. Any inhomogeneity within this region will substantially affect the potential reading to introduce vertical shift in resistivity data. This occurrence affects VES and MT at a different rate. Static shift in both methods increases with surface perturbation in linear and quadratic manners respectively such as shown in Equation 2.9 where f^{VES} and f^{MT} are static shift factors from VES and MT respectively.

$$f^{\text{VES}} = \sqrt{f^{\text{MT}}} \quad (2.9)$$

This indicates that galvanic distortion in MT is substantially greater than in VES by square values. Therefore, the DC measurement from VES is still reliable in correcting MT data. The above equation was employed in a study to recover MT static shift from DC resistivity data by using synthetic and field data (Tripaldi et al., 2010). The multielectrode DC resistivity measurement is utilized to locate the near-surface distortion, quantify the static shift factor and retrieve the actual level of MT impedance. A case study reported that MT data obtained from number of stations recorded different shift magnitudes that are affected by perturbation surficial body and gives erroneous outcomes. VES was conducted on MT stations to produce a successfully resolved static shift problem even for the 2D geometrical body (Stephen et al., 2003). Further inversion using the improved data successfully shown legitimate results.

Another successful integration of VES in MT data for static correction was conducted by Romo et al. (1997), where VES stations cover most MT stations in San Salvador, America. Using Schlumberger electrode array, the apparent resistivity data was employed to remove static shift effect and constraint MT response. Joint inversion of both methods yield an accurate result as compared to individual inversion (Harinarayana, 1999). The result is supported by the existing borehole in the area (Figure 2.16).